



Article

Mechanical Analysis of Flexible Riser with Carbon Fiber Composite Tension Armor

Haichen Zhang , Lili Tong * and Michael Anim Addo

College of Aerospace and Civil Engineering, Harbin Engineering University, Harbin 150001, China; zhc@hrbeu.edu.cn (H.Z.); adoreen64@yahoo.com (M.A.A.)

* Correspondence: tonglili@hrbeu.edu.cn

Abstract: As oil and gas exploration moves to deeper areas of the ocean, the weight of flexible risers becomes an important factor in design. To reduce the weight of flexible risers and ease the load on the offshore platform, this paper presents a cylindrical tensile armor layer made of composite materials that can replace the helical tensile armor layer made of carbon steel. The ACP (pre) of the workbench is used to model the composite tension armor. Firstly, the composite lamination of the tensile armor is discussed. Then, considering the progressive damage theory of composite material, the whole flexible riser is analyzed mechanically and compared with the original flexible riser. The weight of the flexible riser decreases by 9.73 kg/m, and the axial tensile stiffness decreases by 17.1%, while the axial tensile strength increases by 130%. At the same time, the flexible riser can meet the design strength requirements of torsion and bending.

Keywords: flexible riser; tensile armor; carbon fiber; composite tensile armor



Citation: Zhang, H.; Tong, L.; Addo, M.A. Mechanical Analysis of Flexible Riser with Carbon Fiber Composite Tension Armor. *J. Compos. Sci.* **2021**, *5*, 3. <https://dx.doi.org/10.3390/jcs5010003>

Received: 1 December 2020

Accepted: 22 December 2020

Published: 25 December 2020

Publisher's Note: MDPI stays neutral with regard to jurisdictional claims in published maps and institutional affiliations.



Copyright: © 2020 by the authors. Licensee MDPI, Basel, Switzerland. This article is an open access article distributed under the terms and conditions of the Creative Commons Attribution (CC BY) license (<https://creativecommons.org/licenses/by/4.0/>).

1. Introduction

Nowadays, the demand for resources is increasing rapidly in the world, and there are many oil and gas resources in the ocean. Therefore, more and more researchers pay attention to the exploitation of marine resources [1]. A flexible riser is a lifeline for transporting offshore oil and for natural gas resources. The force acting on it during installation and operation is very complex, including bearing tension and internal and external pressure loads. With increases in depth, the suspension weight and fatigue performance of risers have gradually become important. Flexible risers consist of 8 or 9 layers generally, each of which is of a different material, geometry, and function. The carcass and the pressure armor are both self-locking. The carcass is made of AISI304, and the function is to prevent the pipeline from crushing due to hydrostatic pressure or gas accumulation in the annulus of the pipeline. When the axial deformation is too large, the axial stiffness of the riser will be greatly increased after the formation of self-locking [2]. The pressure armor is made of carbon steel strips, and its function is to withstand the stress caused by the fluid pressure in the pipe. Tensile armor is usually made of carbon steel strips that are cross-wound. The cross angle is 30°–55°. It mainly bears the tension, torsional load, and bending moment of flexible pipe. The inner and outer plastic and anti-wear tape are all made of polymers, which provide leak-proof qualities for flexible risers while avoiding direct contact between the armor [3,4].

As oil and gas exploration moves to deeper areas of the ocean, the weight of flexible risers becomes an important factor in the design. To reduce the weight of flexible risers, ease the load on the offshore platform, and alleviate the influence of gravity on risers, the float bowl can be installed outside the risers to provide a certain buoyancy. A common float bowl system currently is the catenary anchor leg mooring (CALM) system. The density of buoy material is as small as possible so that it can provide as large a buoyancy as possible per unit volume. At the same time, it is required to withstand hydrostatic pressure and have lower absorption of water and elasticity modulus so that it can provide stable buoyancy.

However, the buoy increases the volume of the riser. Under waves and current loads, the riser will generate greater motion response and vortex-induced vibration. Ryu [5] used numerical and experimental methods to analyze the time-domain coupling of the CALM system. The free-floating buoy and the buoy with the mooring system were studied, respectively. The frequency–domain analysis model considering the buoy damping force was established, which proved that the damping force plays an important role in the motion response of the buoy. Kang [6] and Hovde [7] studied a deep-water CALM system in West Africa. Kang [6] analyzed the coupled response of the CALM system. It can be seen that the installation of a buoy device reduces the suspension gravity of the riser to a certain extent, but it causes vortex-induced vibration, resulting in greater fatigue damage in the area with the buoy.

Fiber material has high strength weight, which makes the pipeline structure with equivalent structural bearing capacity lighter, and it has higher fatigue and corrosion resistance. Flexible composite pipe (FCP) is made up of reinforced thermoplastic liner coated protective layers [3,4]. Toh et al. [8] analyzed flexible composite pipes and explained that the flexible composite pipes could reduce their weight to alleviate the load-bearing pressure of offshore platforms under the premise of maintaining the mechanical properties by appropriate design. Amaechi et al. [9] discussed the effects of carbon fiber/epoxy (T700), glass fiber/epoxy (S-2), and composite lamination on the safety factor of reinforced thermoplastic flexible composite pipes with an ANSYS ACP (ANSYS Composite PrepPost) module and presented an optimum design method by analyzing the stress of different functional layers. It is more and more common to use FRP (Fiber Reinforced Polymer) material or composite armor instead of metal compression armor and metal tension armor of non-bonded flexible pipe. Technip has developed flexible tubes with four carbon fiber armor layers (CFA). The flexible tube integrated with four carbon fiber armor layers has higher performance and is suitable for light flexible risers, which can reduce or eliminate the need for buoyancy cylinders in ultra-deep-water. Liu [10] developed a model of composite tensile armor layers, introduced it into the whole model, and analyzed the tensile properties of the flexible risers under tensile action. Moreover, for composite cylindrical shells, Wang [11] introduced a reliability-based optimization framework and used it to design filament-wound cylindrical shells with variable angle tows. Almeida et al. [12] evaluated the damage and failure in a carbon fiber reinforced filament wound composite tube and developed a non-linear finite element model, and they found that the model was in good agreement with the experimental structure under external pressure. For progressive damage of composite tubes, Almeida et al. [13], in 2017, used a genetic algorithm to analyze the damage degradation of composite pipes.

There are three main methods to analyze flexible risers: experimental methods, theoretical methods, and numerical methods. De Sousa [14] analyzed the stress of flexible risers under tension, torsion, and internal pressure by an experiment. Because of the high cost of flexible riser experiments, theoretical analysis and numerical simulation analysis have become the prevalent analysis methods. Martindale [15] proposed a theoretical model and used it to investigate the effect of end fittings on the sliding size of steel strips in the tension armor layer of flexible risers. Zhou [16] used a quasi-linear method to establish a theoretical model of risers and analyzed the stress of helical layers under bending. Yoo [2] used Workbench to analyze the ultimate strength of flexible risers. Tang [17] used ABAQUS to analyze the force of flexible risers under combined loads.

There are two kinds of traditional unbonded flexible risers: one is a tensile armor layer made of carbon steel, and the other is a composite flexible riser that is more portable. However, due to its own excessive weight, the former leads to overburden of offshore working platforms, while the latter has poor compressive performance. Therefore, a cylindrical composite tensile armor is proposed in this paper. By taking the structure and function characteristics of flexible risers into account, a numerical model is developed using the finite element model. Considering the progressive damage, firstly, in order to discuss the composite lamination of the tensile armor, the third, fourth and fifth layer models are

used. The whole model is used to predict the mechanical properties of the flexible riser with composite tensile armor. The stiffness and stress of flexible risers under different loads are also calculated. These results are compared with the normal flexible riser with carbon steel helical tensile armor.

2. Theory and Model

2.1. Theory

2.1.1. Elastic Modulus of Composite Material

The composite is composed of matrix material and reinforced material. Assuming that the component materials are uniformly distributed, the macroscopic mechanical behavior of the composite can be regarded as the combined performance of the constituent materials.

In Jones [18], based on the equivalent stress assumption, the elastic parameters of the composite were simplified.

The Young's modulus in the axial (x -axis), circumferential (y -axis) and radial (z -axis) directions as follows:

$$E_x = E_m V_m + E_f V_f$$

$$E_y = E_m (1 - V_1) + \frac{E_m E_f V_1}{\frac{E_m V_f}{V_1} + E_f \left(1 - \frac{V_f}{V_1}\right)}$$

$$E_z = E_m \left(1 - \frac{V_f}{V_1}\right) + \frac{E_m E_f \frac{V_f}{V_1}}{E_m V_f + E_f (1 - V_1)}$$

$$E_z = E_m \left(1 - \frac{V_f}{V_1}\right) + \frac{E_m E_f \frac{V_f}{V_1}}{E_m V_f + E_f (1 - V_1)}$$

The Poisson's ratio is as follows:

$$\mu_{xy} = \mu_{xz} = \mu_f V_f + \mu_m V_m$$

$$\mu_{yz} = \frac{\mu_f V_f + \mu_m \frac{E_f}{E_m} (V_1 - V_f)}{\frac{V_f}{V_1} + \frac{E_f}{E_m} \left(1 - \frac{V_f}{V_1}\right)} + \mu_m V_2$$

The shear modulus is as follows:

$$G_{xy} = \frac{G_f G_m \frac{V_f}{V_1}}{G_m V_1 + G_f V_2} + G_m \left(1 - \frac{V_f}{V_1}\right)$$

$$G_{yz} = \frac{G_f G_m V_1}{G_m \frac{V_f}{V_1} + G_f \left(1 - \frac{V_f}{V_1}\right)} + G_m V_2$$

$$G_{xz} = \frac{G_f G_m \frac{V_f}{V_1}}{G_m V_1 + G_f V_2} + G_m \left(1 - \frac{V_f}{V_1}\right)$$

2.1.2. Analytical Model of Unbonded Flexible Riser

When establishing the analysis model, the flexible riser is usually divided into a spiral layer and cylindrical layer. The cylindrical layer consists of an anti-wear layer and internal and external plastic layers. The helical layer consists of a tensile armor layer, a compressive armor layer, and a carcass. In this paper, the carbon fiber tensile armor is considered as a cylindrical layer. Limited by the length of this paper, only the establishment of the cylindrical layer model is introduced.

The polymer material is considered to be linearly elastic and isotropic. The thick-walled cylinder theories are used to analyze the cylindrical layer [2,18,19].

Stress and deformation are shown in Figure 1, where

$$\epsilon_1 = \frac{\mu_z}{L}; \epsilon_2 = \frac{\partial \mu_R}{\partial R}; \epsilon_3 = \frac{\mu_R}{R}; \gamma_{12} = R \frac{\mu_\theta}{L}$$

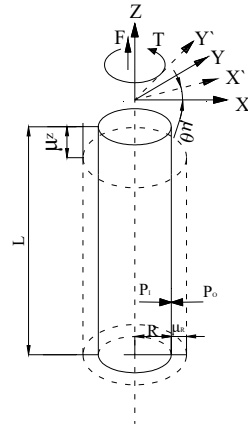


Figure 1. Loads and deformations of cylindrical layer.

This external potential energy [20] is calculated as follows:

$$U_e = P_I \Delta V_I - P_o \Delta V_o + F \mu_z + T \mu_\theta \tag{1}$$

The strain energy of the cylindrical layer is

$$U_c = \frac{1}{2} \int_v (\sigma_1 \epsilon_1 + \sigma_2 \epsilon_2 + \sigma_3 \epsilon_3 + \tau_{12} \gamma_{12}) dv \tag{2}$$

In order to simplify the calculation process, it is necessary to simplify the parameters.

$$X_Z = \frac{\mu_z}{L}; X_\theta = R \frac{\mu_\theta}{L}; X_{\varphi I} = \frac{\mu_{R_I}}{R_I}; X_{\varphi O} = \frac{\mu_{R_O}}{R_O}$$

The total potential energy of the cylindrical layer is as follows, and the strain energy U_c is obtained from Equation (2); the external potential energy U is obtained from Equation (1):

$$\Pi_c = U - U_e$$

Taking the variation of the total potential energy and making it equal to 0, the equation is as follows:

$$\begin{bmatrix} K_{c11} & K_{c12} & K_{c13} & K_{c14} \\ K_{c21} & K_{c22} & K_{c23} & K_{c24} \\ K_{c31} & K_{c32} & K_{c33} & K_{c34} \\ K_{c41} & K_{c42} & K_{c43} & K_{c44} \end{bmatrix} \begin{bmatrix} X_Z \\ X_{\varphi I} \\ X_{\varphi O} \\ X_\theta \end{bmatrix} = \begin{bmatrix} F + \pi P_I R_I^2 - \pi P_O R_O^2 \\ 2\pi P_I R_I^2 \\ -2\pi P_O R_O^2 \\ T \end{bmatrix}$$

2.1.3. Failure Criteria for Composites

When the matrix of the composites is damaged, and the fibers are not broken, the composites can still bear the load. Therefore, the strength degradation caused by matrix failure should be considered in the mechanical analysis.

The failure process of composites is complex, and the damage forms are various. There are many failure criteria for composites. The Hashin failure criterion is based on the material parameter degradation criterion, and the cumulative damage of a single-layer plate is considered. The Hashin criterion is used to judge the composite tensile armor [21,22]. The results of Hashin criteria are composed of four separate failure modes [23]:

The tensile fibers mode $\sigma_{11} > 0$ is

$$\left(\frac{\sigma_{11}}{T_{11}}\right)^2 + \left(\frac{\tau_{12}^2 + \tau_{13}^2}{S_{12}^2}\right) = 1$$

Compression fibers mode $\sigma_{11} < 0$ is

$$-\frac{\sigma_{11}}{C_{12}} = 1$$

Tensile matrix mode $\sigma_{22} + \sigma_{33} > 0$ is

$$\left(\frac{\sigma_{22} + \sigma_{33}}{T_{22}}\right)^2 + \frac{(\tau_{23}^2 - \sigma_{22}\sigma_{23})}{S_{23}^2} + \frac{(\tau_{12}^2 + \tau_{13}^2)}{S_{12}^2} = 1$$

Compression matrix mode $\sigma_{22} + \sigma_{33} < 0$ is

$$\frac{1}{C_{22}} \left[\left(\frac{C_{22}}{2S_{23}}\right)^2 \right] (\sigma_{22} + \sigma_{33}) + \frac{(\sigma_{22} + \sigma_{33})^2}{4S_{23}^2} + \frac{(\tau_{23}^2 - \sigma_{22}\sigma_{23})}{S_{23}^2} + \frac{(\tau_{12}^2 + \tau_{13}^2)}{S_{12}^2} = 1$$

The matrix stiffness degradation criterion used in this paper is as follows [24]:

Tensile cracking of matrix:

$$E_{22} = 0.2E_{22}, G_{12} = 0.2G_{12}, G_{23} = 0.2G_{23}$$

Compression cracking matrix:

$$E_{22} = 0.4E_{22}, G_{12} = 0.4G_{12}, G_{23} = 0.4G_{23}$$

Fiber shear matrix:

$$G_{12} = v_{12} = 0$$

2.1.4. Contact Formulation

Coulomb type friction between bodies is

$$F = \mu \times R$$

For the contact of faces, pure penalty or augmented Lagrange formulations can be used.

The main difference between pure penalty and augmented Lagrange methods is that augmented Lagrange includes the contact force (pressure) calculations:

Pure Penalty:

$$F = K_N \times x_p$$

Augmented Lagrange:

$$F = K_N \times x_p + \lambda$$

where K_N is the contact stiffness, x_p is the penetration, and λ is the Lagrange multiplier.

2.2. Finite Element Model

Three cases of flexible risers are used in this paper, as shown in Table 1. The first case (case 1) is flexible risers with a carbon steel structure, as seen in Figure 2, and the second case (case 2) is flexible tubes with four carbon fiber armor layers (CFA) developed by Technip. The third case (case 3) is flexible risers with a carbon fiber composite tensile armor layer.

Table 1. Three cases in this paper.

Case	Amount of Layer	Tensile Armor	Figure
case 1	8	2 carbon steel tensile armor	As shown in Figure 2
case 2	12	4 spiral carbon fiber composite tensile armor	Technip and reference
case 3	8	2 cylindrical carbon fiber composite tensile armor	As shown in Figure 3

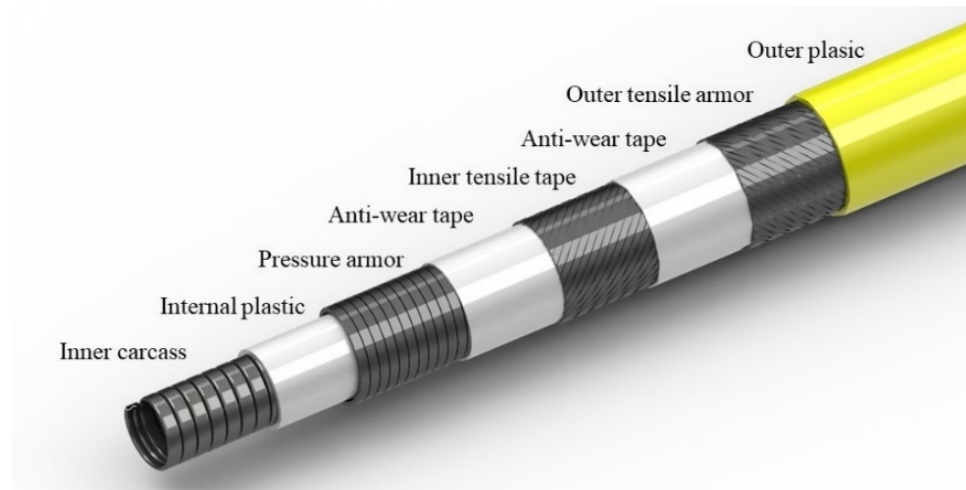


Figure 2. Flexible riser with carbon fiber composite tension armor.

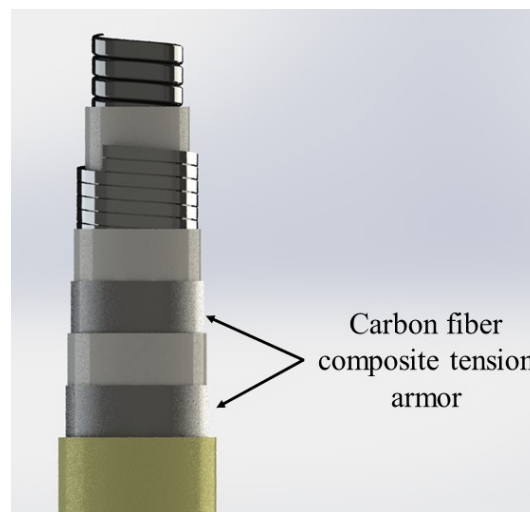


Figure 3. Flexible riser with eight layers.

2.2.1. Model Parameters

In this paper, the geometrical and material parameters of the flexible risers are given in the experimental papers on non-bonded flexible risers published by de Sousa [14], as shown in Tables 2 and 3.

Table 2. Geometric parameters of flexible risers tested.

No.	Type	Material	Inner Radius (mm)	External Radius (mm)	Angle	Thickness (mm)	Moment of Inertia (mm ⁴)	Width (mm)
1	Carcass	AISI 304	31.75	35.25	+87.6° (1)	3.5	23.1	5.6
2	Internal plastic	Polyamide 11	35.25	40.25	-	5.0	-	-
3	Pressure armor	Carbon steel	40.25	46.85	85.6°	6.6	173.4	8.73
4	Anti-wear tape	Polyamide 11	46.85	48.85	-	2	-	-
5	Internal tensile armor	Carbon steel	48.85	51.35	+30° (32)	2.5	-	8
6	Anti-wear tape	Polyamide 11	51.35	52.85	-	1.5	-	-
7	Outer tensile armor	Carbon steel	52.85	55.35	-30° (34)	2.5	-	8
8	Fabric tape	Polyamide	55.35	55.85	-	0.5	-	-
9	Out plastic	Polyamide	55.85	60.85	-	5.0	-	-

Table 3. Material parameters.

Material	Density (kg/m ²)	E (MPa)	ν
AISI 304	7930	205 × 10 ³	0.3
Polyamide 11	803	345	0.3
Carbon steel	7820	205 × 10 ³	0.3
Polyamide (eighth)	803	345	0.3
Polyamide (ninth)	803	215	0.3

The ultimate strength of carbon steel is 750–800 MPa [3,4].

Details of the material properties used in this investigation are presented in Table 4.

Table 4. Mechanical properties of carbon fiber reinforced composites.

Carbon fiber/Epoxy(T700)	Density (kg/m ²)	1580	σ ₁ ^C (MPa)	900
	E1 (GPa)	120	σ ₂ ^T (MPa)	20
	E2 =E3 (GPa)	10	σ ₂ ^C (MPa)	240
	G12 = G13 (GPa)	5	τ ₁₂ (MPa)	18
	G23 (GPa)	5	ν ₁₂ = ν ₁₃	0.2
	σ ₁ ^T (MPa)	1800	ν ₂₃	0.27

Flexible pipes usually have high axial stiffness, and their allowable elongation is about 0.5–1.5% [3,4]. The design must satisfy the requirements of the required axial stiffness and torsional properties and control the clearance between metal wires.

The composite lamination of the tensile armor could be designed by the stress characteristics of the tensile armor and the mechanical properties of the composite material. The direction of the pipe axis is taken as the reference direction, and the composite tension armor includes 0° angle fibers, 30° angle fibers, and 90° angle fibers. The axial load is mainly supported by the fibers in the angle of 0° and 30°. The torsion load is mainly supported by the fibers in the angle of 30° in order to deal with the phenomenon of “birdcage” caused by the axial pressure mentioned in references [2,17,25,26], and to maintain the integrity of the composite tensile armor of 90 angle directional fibers. The sequence and orientation of composite tensile armor are shown in Table 5.

Table 5. The sequence and orientation of composite tensile armor.

Name	Thickness (mm)	Sequence and Orientation
Internal tensile armor	2.4	[90 ₂ , α ₂ , 0 ₆ , 0 ₆ , -α ₂ , 90 ₂]
Outer tensile armor	2.4	[90 ₂ , -α ₂ , 0 ₆ , 0 ₆ , α ₂ , 90 ₂]

2.2.2. Flexible Riser Model

The structure of a flexible riser, which is very complex, can be divided into the spiral layer (carcass, compressive armor, tensile armor) and cylindrical layer (inner and outer sheath layer, anti-wear layer). In order to enhance the convergence, improve the computational efficiency, and save the computational cost, the shell element is used to simulate the cylindrical structure in this paper. The self-locking carcass and the pressure armor are simplified as an anisotropic cylindrical shell [27].

According to the structure and material parameters in Tables 4 and 5, a three-dimensional model of flexible pipe with a length of 1 m was established firstly. Then, the model was introduced to the ANSYS workbench for mesh generation. The mesh of tensile armor size was 10 mm, and other layers were 15 mm. The tensile armor layer and the overall model are shown in Figure 4.



Figure 4. Mesh of flexible riser model. (a) Tensile armor layer, (b) Overall model

2.2.3. Composite Tension Armor

The setup flows as follows: setting the material properties → establishment of reference coordinate system → setting the angle of the fiber. The direction of the reference axis in this paper is the direction of the tube axis, and the normal direction is the thickness direction of the tensile armor, as shown in Figure 5a. The yellow arrow indicates the direction of the fiber reference, and the purple arrow represents the normal direction. The direction of the fiber layer in 0° direction is shown in Figure 5b.

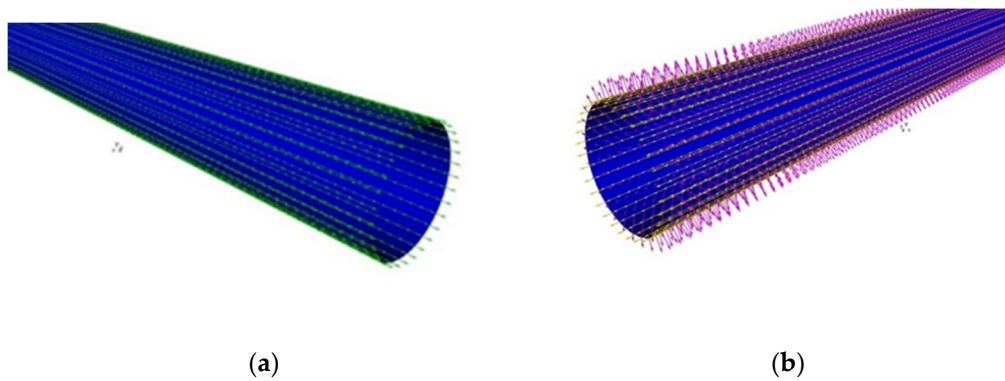


Figure 5. Definition of composite tensile armor. (a) Reference axis, (b) 0° fiber.

2.2.4. Contact

Contact mechanics is a considerable challenge when creating numerical models. The distribution of normal and tangential force, penetration and local constraint conditions, and variation in material and mechanical properties of each layer present difficulties in obtaining solution convergence and successful modeling outcomes [28,29].

To converge the calculation and ensure the accuracy of the results, the augmented Lagrange method is chosen in this paper. The difference between simulation using solid element and shell element is discussed in [2]. The stiffness calculated by the shell element

is considered to be slightly larger, however, when the intrusion tolerance of the contact surface is 5%; the calculated stiffness of the shell element is slightly less than that of the solid element, but the difference can be neglected. With respect to the tangential contact, the friction coefficient used in Yoo [2] and Asousa [14] is 0.1, and Tang [17] is 0.2. The friction coefficient used in this paper is 0.1.

2.2.5. Boundary Conditions and Load

According to [3], the design of the tensile armor of flexible risers must meet the requirements of the required axial strength and any torsional properties. In this paper, we set fixed boundary conditions at one end of the pipe. At the other end, axial loads and torsional loads were applied. External pressure was applied to the outer surface of the plastic. For bending cases, the loads and constraints are shown in Figure 6.

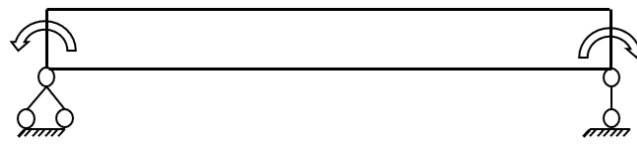


Figure 6. Boundary conditions of bending condition.

3. Results

3.1. The Composite Lamination of the Tensile Armor

It was proved in [15,27] that under the action of axial tensile load, the carcass, inner plastic, and compressive armor do not affect the stress analysis. The fourth, fifth, and sixth layers structures were only analyzed. To simulate the action of carcass and compressive armor against internal and external pressure, radial restraint was applied to the inner surface of the fourth layer. The stress distribution diagram of 0° angle fiber in composite tensile armor is shown in Figure 7.

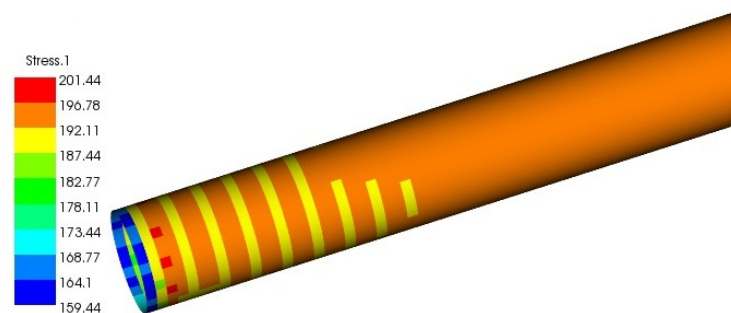


Figure 7. The stress of 0° fiber.

The relationship between the axial deformation and the axial tension is shown in Figure 8a. The stiffness of the whole riser was obtained by dividing the deformation by the load. Moreover, when the axial tension was small, the relationship between tension and deformation was linear, and with increases in tension, the axial stiffness decreased. The reason is that the elastic modulus of composites was reduced, according to the failure criteria and strength degradation criteria explained in Section 2.1.2. Figure 8b shows the relationship between the torsion angle and torque. As can be seen from the figure, the relationship was linear. When α was 30° , 45° , or 60° , the torsional stiffness of the cylindrical tension armor was the largest. Therefore, the α in this paper was 30° .

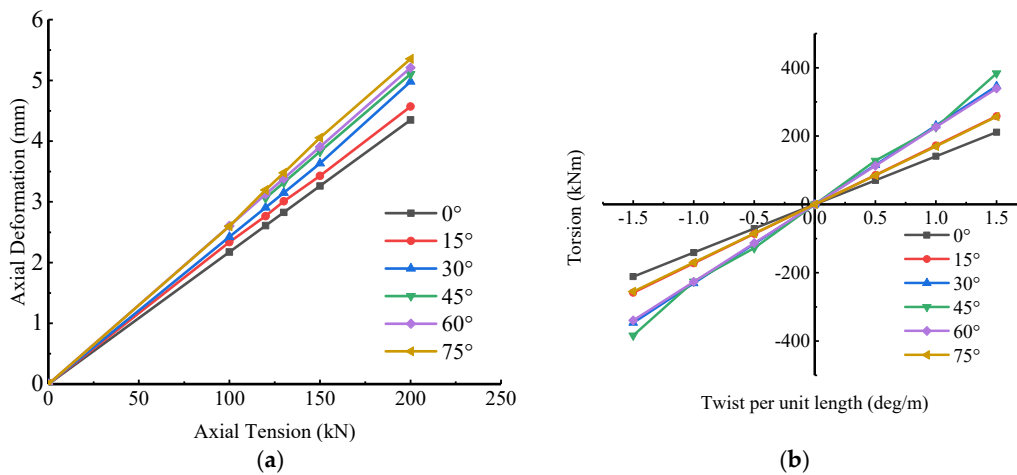


Figure 8. Displacement of flexible riser under tension and torsion. (a) Axial deformation versus tension per unit length, (b) twist versus torsion per unit length.

3.2. Pure Axial Tensile

The axial deformation was applied at the free end, and the axial tension was measured by the reaction force at the fixed end. The stress of the tensile armor was observed until the strength limit of the material. The relationship between axial tension and deformation of two cases of flexible risers is shown in Figure 9a, and the stress of tensile armor versus axial tension is shown in Figure 9b.

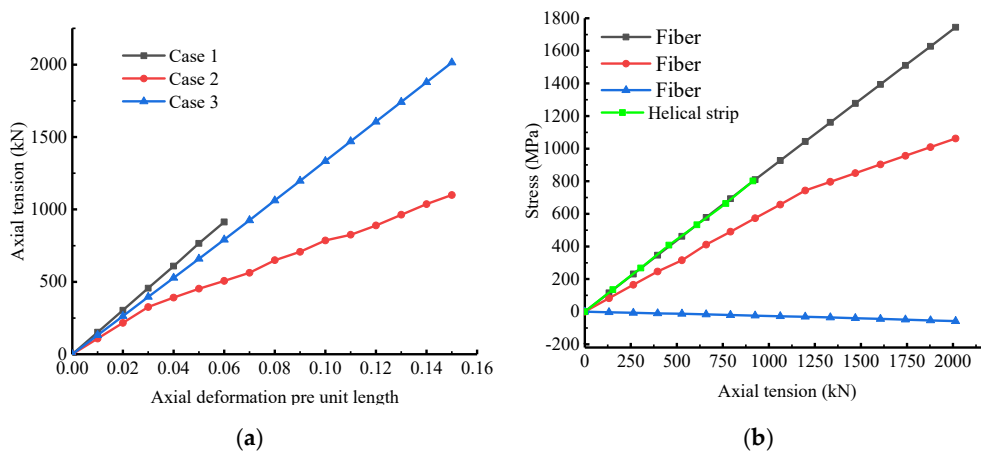


Figure 9. Axial deformation versus tension per unit length and stress of tensile armor. (a) Axial deformation versus tension per unit length; (b) the stress of tensile armor versus tension per unit length.

As shown in Figure 9a, the results of case 1 were compared with the results of an experiment in [14]. The simulation error of the model for the flexible riser was less than 5%, which proves the availability of the model. It can be seen from the figure that the relationship between the axial tension and the axial deformation of flexible risers was linear. However, when the load increased, case 2 and case 3 had a nonlinear relationship. The reason is that the matrix was cracked by the tension when the displacement was 10 mm. The axial tension of flexible risers in case 2 was smaller than those in case 3 with the same axial deformation. This indicates that the overall tensile strength of the flexible risers in case 2 was lower than those in case 3. This indicates that the overall stiffness of the flexible riser with the composite tensile layer was lower than that with the carbon steel tensile layer, and the overall stiffness of the flexible riser with cylindrical carbon fiber tensile armor layers in case 3 was higher than the flexible riser with four carbon fiber armor layers.

Figure 9b shows the stress of helical strips in case 1 and fiber in case 3. As seen in this figure, the tensile load in case 2 was mainly borne by fibers in the direction of 0 and 30. The fiber stress in the angle of 0° increased linearly with the increase of load. When the tension was greater than 1197 kN, the rate of increase of the fiber stress in the angle of 30° decreased. When the axial deformation was 6 mm, the helical strip stress of case 1 was 800 MPa, which is the ultimate strength of carbon steel. When the load turned to 2000 kN, the axial displacement was 15 mm, and the stress of the fiber at 90° was 1744 MPa which is the ultimate strength of carbon fiber. Comparing case 1 with case 3, the ultimate tensile strength of flexible risers with cylindrical composite tensile armor layers improved greatly, about one time.

3.3. Tension and External Pressure

The flexible riser was mainly subjected to the combined load (internal and external pressure and tension) during its operation and installation. Therefore, this section discusses the effect of external pressure on axial stiffness. Firstly, the different external pressure was applied on the outer surface of the flexible riser, and then the axial displacement was applied at the free end. The reaction force at the fixed end was the axial tension.

Figure 10a shows the variation of axial tension of the flexible riser with external pressure. It can be seen from the figure that the axial stiffness of the flexible riser decreased under external pressure. Compared with case 1, case 2, and case 3, the effect of external pressure on the overall axial tensile stiffness of the flexible riser with cylinder carbon fiber tensile armor (in case 3) was smaller than the risers with helical carbon steel tensile armor (in case 1), and the effect on flexible risers with four carbon fiber armors (in case 2) was the biggest. This suggests that the effect is enhanced when the form of the tensile armor layer is helical.

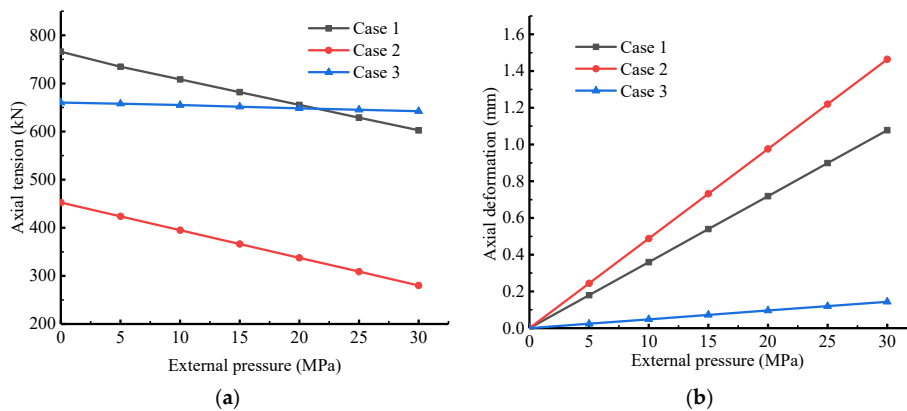


Figure 10. Influence of external pressure on axial deformation. (a) Axial tension versus external pressure per unit length, (b) axial deformation versus external pressure per unit length.

With the increase of external pressure, the reduction of axial load is linear [14]. The flexible riser itself caused axial deformation under external pressure. Figure 10b shows the axial deformation under pure external pressure. As seen in Figure 10, the flexible riser in case 1 produced 1.08 mm axial deformation under 30 MPa external pressure, and the riser in case 2 produced 1.436 mm; the riser in case 2 only produced 0.144 mm axial deformation under the same external pressure. This is the reason why the reduction rate of axial stiffness is different under external pressure.

3.4. Torque

The allowable torsion deformation of flexible pipe is 0.5–1.5 (deg/m) [4]. The flexible riser was fixed at one end, and torsional displacement was applied at the other end. Clockwise was positive (the same winding direction as the outer tension armor layer), and counterclockwise was negative. The results are shown in Figure 11a.

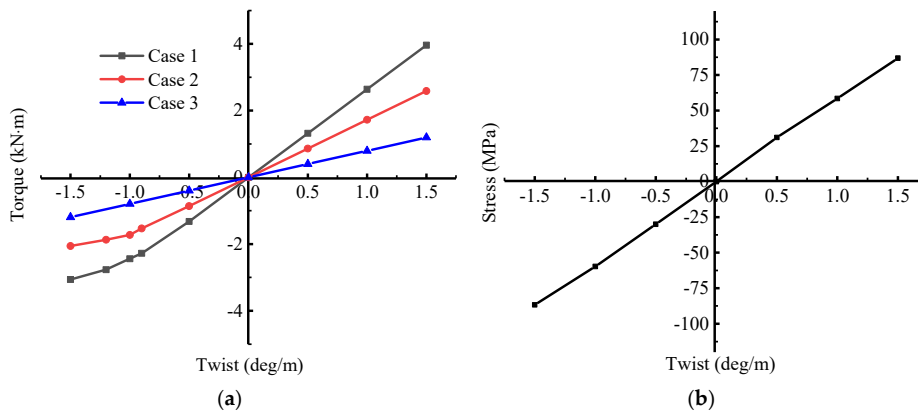


Figure 11. Torque and stress of 0° fiber versus twist per unit length. (a) Torque versus twist per unit length; (b) stress of 30° fiber versus twist per unit length.

As can be seen from this figure, when the torsion angle was positive, the torsion and the torsion moment of the two flexible risers showed a linear relationship. When the torsion was negative, the torsional stiffness of the flexible riser in case 1 decreased with the increase of the torsion, which was caused by the phenomenon of separation between layers of the pipeline. In case 2, the torsional stiffness of flexible riser did not change due to the different directions of the torsional angle. Overall, the torsional stiffness of flexible risers with composite tension armor was reduced by three times. Within the allowable torsion angle of the flexible riser (0.5–1.5 deg/m), the composite tensile armor did not show any damage.

The stress of each layer’s fiber in the composite tensile armor can be obtained from the post module. It can be seen that when the flexible riser was twisted at the free end, the fibers in the composite tensile armor layer were the major fibers, and the stress was high, but the fibers in the direction of 0 and 90 were very low. Figure 12 shows the stress of fiber at the angle of 30° under the twist of 1.5 deg/m at the free end. Figure 11b is the stress of 30° fibers varying with the torsion angle of the free end. It can be seen that the relationship between stress of 30° fibers and twist of the free end is linear.

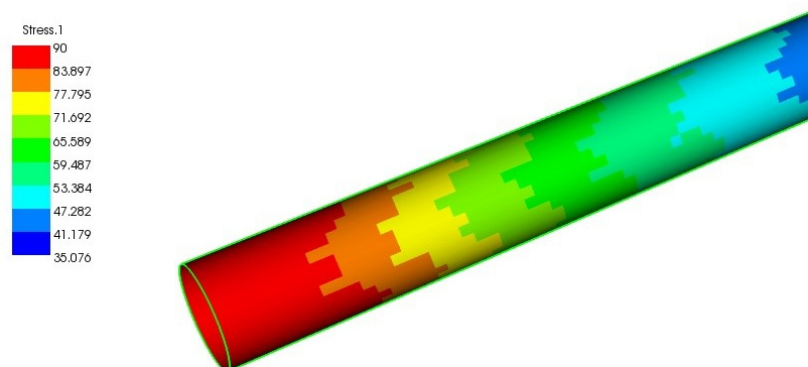


Figure 12. The stress of 30° fiber under 1.5 deg/m twist.

3.5. Bending

The flexible riser bends in the process of transportation, installation, and operation; as a result, the composite tension armor layer needs to meet the requirements of the flexible riser’s bending deformation.

As shown in Figure 13a,b, both the flexible risers in the two cases could be divided into three phases during bending: non-slip phase, partial slip phase, and complete slip phase. Furthermore, the bending stiffness of the flexible riser in case 2 was higher than that in case 1. From the non-slip phase to the slip phase, the change of bending stiffness in case 2 had a smaller change than that in case 1.

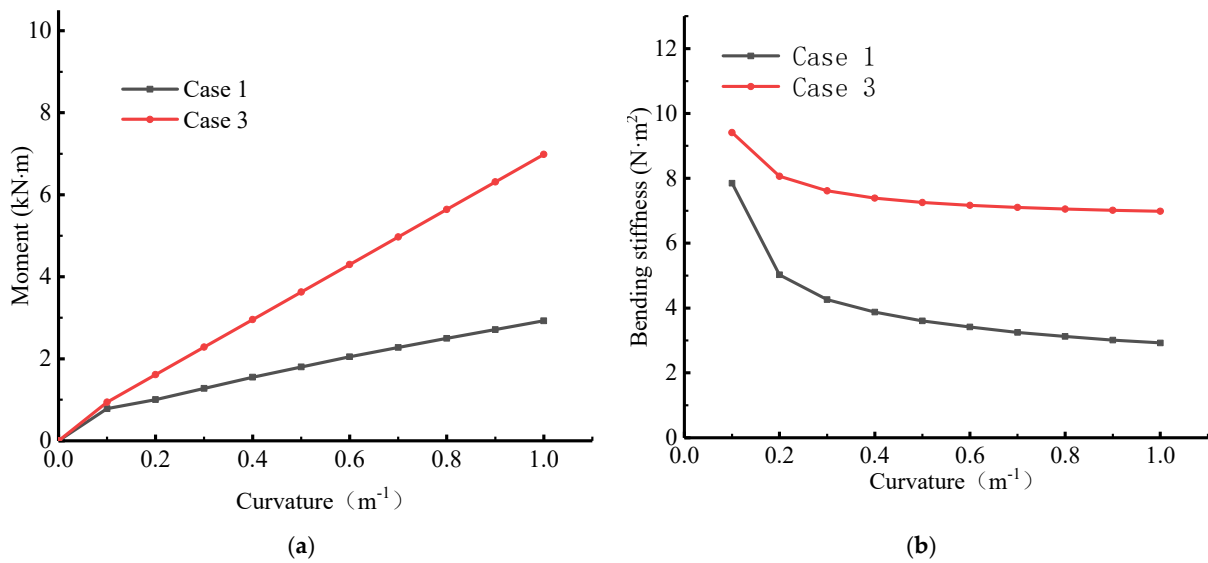


Figure 13. Bending moment and stiffness. (a) Moment–curvature; (b) bending stiffness.

Figure 14 shows the fiber stress of the composite tensile armor layer when the riser was bending. Figure 14a shows the fiber stress of the composite tensile armor layer during bending deformation of the riser. For the most part, 0 and 30-degree fibers were working. With the increase of curvature, the stress increased linearly. The lamination of the composite tensile armor layer was [90₂, 30₂, 0₆, 0₆, -30₂, 90₂]. Figure 14b shows the stress of all fibers in the angle of 0° in the composite tensile armor when the curvature was 1 rad/m. The layer numbers from 1 to 12 indicate from inside to the outside of the diameter. It can be found from the figure that the stress of the 0° fibers in the two composite tensile armors increased with the layer number. According to the failure criterion in Section 2.1.2, the failure of composite tension armor is matrix compression and shear failure. Figure 15 shows the stress of fibers in the angle of 0° and 30°. The maximum stress value of 0° fiber of composite tensile armor was 889 MPa, which did not reach the tensile strength of the carbon fiber, and there was no tensile fracture phenomenon of the fiber. It shows that the flexible pipe with composite tensile armor can withstand bending deformation without failure and meet the design requirements.

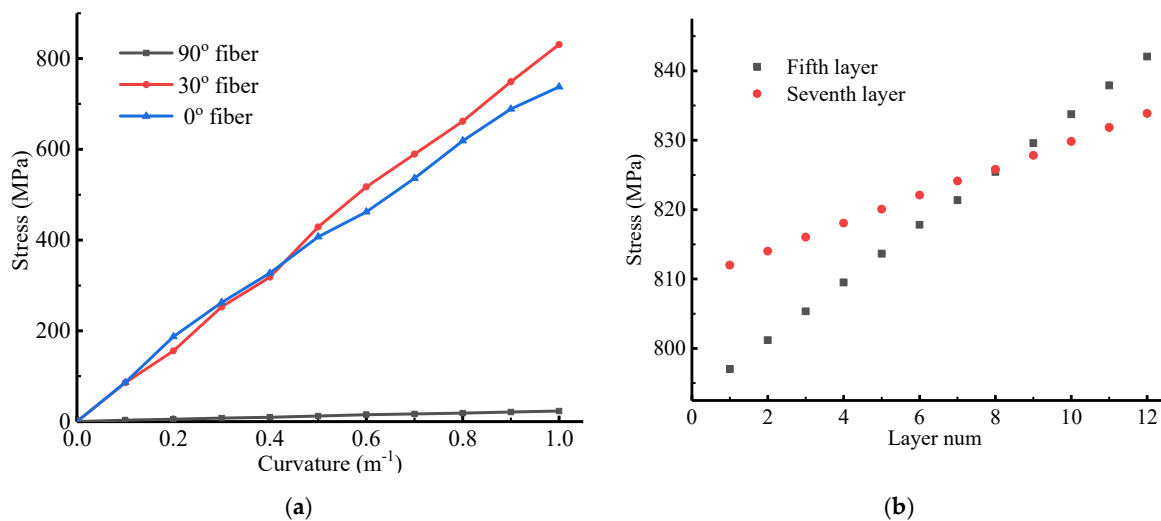


Figure 14. Fiber stress of composite tension armor. (a) Fiber stress versus curvature per unit length; (b) the stress of fiber at 0° versus curvature per unit length.

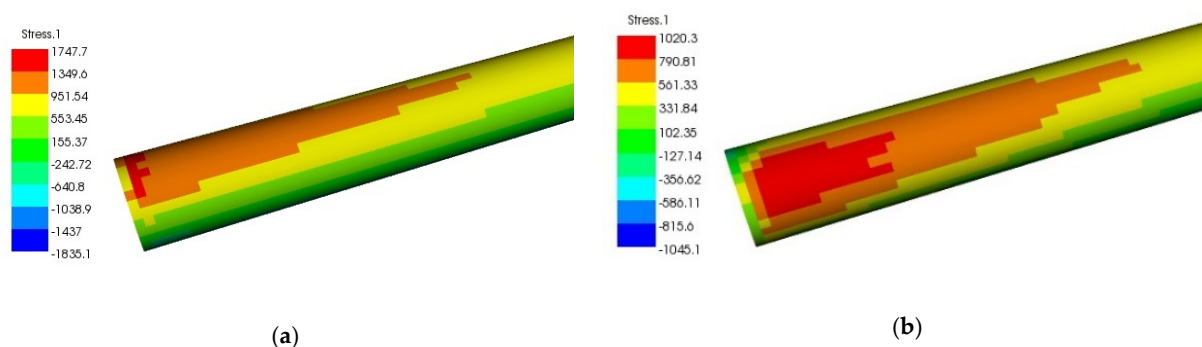


Figure 15. Stress state of fiber. (a) Stress fiber in 0° angle; (b) stress fiber in 30° angle.

4. Conclusions

To reduce the self-weight of a flexible riser, a cylinder composite tensile armor is proposed in this paper. From the analysis and calculation, the conclusions are as follows:

The suitable laminate for the composite tensile armor is $[90_2, 30_2, 0_6, 0_6, -30_2, 90_2]$. The weight of the flexible riser with composite armor decreased by 9.73%. It can effectively reduce the burden of offshore platforms.

The composite matrix will be damaged in the process of use, but the fibers can continue to function. Therefore, the flexible riser with composite tensile armor sometimes experiences the phenomenon of stiffness reduction in the process of loading. The stiffness and strength of flexible risers with cylinder composite tensile armor changed; the tensile stiffness was reduced by 17%, the torsional stiffness was reduced by 60%, and the flexural stiffness was increased by 130%. Moreover, the effect of external pressure on the overall tensile stiffness was significantly reduced. In terms of strength, the tensile strength of flexible risers increased by 150%. At the same time, flexible risers could also withstand torsional and bending deformations within a specified range.

Author Contributions: Conceptualization, H.Z. and L.T.; methodology, H.Z. and L.T.; software, H.Z.; validation, H.Z., L.T., and M.A.A.; formal analysis, H.Z. and L.T.; investigation, H.Z.; resources, H.Z. and L.T.; data curation, H.Z. and L.T.; writing—original draft preparation, H.Z. and M.A.A.; writing—review and editing, H.Z., L.T., and M.A.A.; visualization, H.Z.; supervision, L.T.; All authors have read and agreed to the published version of the manuscript.

Funding: This research received no external funding.

Informed Consent Statement: Informed consent was obtained from all subjects involved in the study.

Data Availability Statement: The data presented in this study are available on request from the corresponding author. The data are not publicly available due to privacy or ethical restrictions.

Acknowledgments: The authors are grateful to Lili Tong for her help in the analysis and writing of this paper and Michael Anim Addo for his help in grammar and writing.

Conflicts of Interest: We declare that we have no financial and personal relationships with other people or organizations that can inappropriately influence our work, and that there is no professional or other personal interest of any nature or kind in any product, service, and/or company that could be construed as influencing the position presented in, or the review of, the manuscript entitled.

References

1. Dudley, B. *BP Energy Outlook*; BP Amoco: London, UK, 2018.
2. Yoo, D.-H.; Jang, B.-S.; Yim, K.-H. Nonlinear finite element analysis of failure modes and ultimate strength of flexible pipes. *Mar. Struct.* **2017**, *54*, 50–72. [[CrossRef](#)]
3. API. *Recommended Practice for Flexible Pipe*, 5th ed.; API RP 17B; American Petroleum Institute: Washington, DC, USA, 2014.
4. API. *Specification for Unbounded Flexible Pipe, APIA Specification 17*, 4th ed.; American Petroleum Institute: Washington, DC, USA, 2014.
5. Ryu, S.; Duggal, A.S.; Heyl, C.N.; Liu, Y. Prediction of deepwater oil offloading buoy response and experimental validation. *Int. J. Offshore Polar Eng.* **2006**, *16*, 290–296.

6. Kang, Y.; Sun, L.; Kang, Z.; Chai, S. Coupled analysis of FPSO and CALM buoy offloading system in West Africa. In Proceedings of the ASME 2014 33rd International Conference on Ocean, Offshore and Arctic Engineering, San Francisco, CA, USA, 8–13 June 2014.
7. Hovde, G.O.; Kaalstad, J.P.; Skjaastad, O. Offloading in Deep and Ultradeep Water—Main Drivers and Need for Improved Systems. In Proceedings of the Offshore Technology Conference, Houston, TX, USA, 2 May 2005.
8. Toh, W.; Bin Tan, L.; Jaiman, R.K.; Tay, T.E.; Tan, V. A comprehensive study on composite risers: Material solution, local end fitting design and global response. *Mar. Struct.* **2018**, *61*, 155–169. [[CrossRef](#)]
9. Amaechi, C.V.; Gillett, N.; Odijie, A.C.; Hou, X.; Ye, J. Composite risers for deep waters using a numerical modelling approach. *Compos. Struct.* **2019**, *210*, 486–499. [[CrossRef](#)]
10. Liu, Q.; Xue, H.; Tang, W.; Yuan, Y. Theoretical and numerical methods to predict the behaviour of unbonded flexible riser with composite armour layers subjected to axial tension. *Ocean Eng.* **2020**, *199*, 107038. [[CrossRef](#)]
11. Wang, Z.; Almeida, J.H.S., Jr.; St-Pierre, L.; Wang, Z.; Castro, S.G. Reliability-based buckling optimization with an accelerated Kriging metamodel for filament-wound variable angle tow composite cylinders. *Compos. Struct.* **2020**, *254*, 112821. [[CrossRef](#)]
12. Almeida, J.H.S.; Ribeiro, M.L.; Tita, V.; Amico, S.C. Damage and failure in carbon/epoxy filament wound composite tubes under external pressure: Experimental and numerical approaches. *Mater. Des.* **2016**, *96*, 431–438. [[CrossRef](#)]
13. Almeida, J.H.S.; Ribeiro, M.L.; Almeida, J.H.S.; Amico, S.C. Stacking sequence optimization in composite tubes under internal pressure based on genetic algorithm accounting for progressive damage. *Compos. Struct.* **2017**, *178*, 20–26. [[CrossRef](#)]
14. De Sousa, J.R.; Magluta, C.; Roitman, N.; Vargas-Londono, T.; Campello, G. A Study on the Response of a Flexible Pipe to Combined Axisymmetric Loads. In Proceedings of the ASME 2013 32nd International Conference on Ocean: Offshore and Arctic Engineering, Nantes, France, 9–14 June 2013.
15. Out, J.; Von Morgen, B. Slippage of helical reinforcing on a bent cylinder. *Eng. Struct.* **1997**, *19*, 507–515. [[CrossRef](#)]
16. Zhou, Y.; Vaz, M.A. A quasi-linear method for frictional model in helical layers of bent flexible risers. *Mar. Struct.* **2017**, *51*, 152–173. [[CrossRef](#)]
17. Tang, L.; He, W.; Zhu, X.; Zhou, Y. Mechanical analysis of un-bonded flexible pipe tensile armor under combined loads. *Int. J. Press. Vessel. Pip.* **2019**, *171*, 217–223. [[CrossRef](#)]
18. Bai, Y.; Lu, Y.; Cheng, P. Analytical prediction of umbilical behavior under combined tension and internal pressure. *Ocean Eng.* **2015**, *109*, 135–144. [[CrossRef](#)]
19. Merino, H.E.M.; de Sousa, J.R.M.; Magluta, C.; Roitman, N. Numerical and Experimental Study of a Flexible Pipe under Torsion. In Proceedings of the International Conference on Offshore Mechanics and Arctic Engineering, Shanghai, China, 6–11 June 2010; pp. 911–922.
20. Bussetta, P.; Marceau, D.; Ponthot, J.-P. The adapted augmented Lagrangian method: A new method for the resolution of the mechanical frictional contact problem. *Comput. Mech.* **2011**, *49*, 259–275. [[CrossRef](#)]
21. Gu, J.; Chen, P. Some modifications of Hashin's failure criteria for unidirectional composite materials. *Compos. Struct.* **2017**, *182*, 143–152. [[CrossRef](#)]
22. Tserpes, K.I.; Papanikos, P.; Kermanidis, T. A three-dimensional progressive damage model for bolted joints in composite laminates subjected to tensile loading. *Fatigue Fract. Eng. Mater. Struct.* **2001**, *24*, 663–675. [[CrossRef](#)]
23. Zhang, X.; Gou, R.; Yang, W.; Chang, X. Vortex-induced vibration dynamics of a flexible fluid-conveying marine riser subjected to axial harmonic tension. *J. Braz. Soc. Mech. Sci. Eng.* **2018**, *40*, 365. [[CrossRef](#)]
24. Liu, P.; Gu, Z.; Yang, Y.; Peng, X. A nonlocal finite element model for progressive failure analysis of composite laminates. *Compos. Part B Eng.* **2016**, *86*, 178–196. [[CrossRef](#)]
25. Novitsky, A.; Gray, F. Flexible and Rigid Pipe Solutions in the Development of Ultra-Deepwater Fields. *Int. Conf. Offshore Mech. Arct. Eng.* **2003**, 36827, 755–770.
26. Vaz, M.; Rizzo, N. A finite element model for flexible pipe armor wire instability. *Mar. Struct.* **2011**, *24*, 275–291. [[CrossRef](#)]
27. Li, X.; Jiang, X.; Hopman, H. A strain energy-based equivalent layer method for the prediction of critical collapse pressure of flexible risers. *Ocean Eng.* **2018**, *164*, 248–255. [[CrossRef](#)]
28. Ebrahimi, A.; Kenny, S.; Hussein, A. Finite Element Investigation on the Tensile Armor Wire Response of Flexible Pipe for Axisymmetric Loading Conditions Using an Implicit Solver. *J. Offshore Mech. Arct. Eng.* **2018**, *140*, 041402. [[CrossRef](#)]
29. De Sousa, J.R.; Magluta, C.; Roitman, N.; Ellwanger, G.B.; Lima, E.C.; Papaleo, A. On the response of flexible risers to loads imposed by hydraulic collars. *Appl. Ocean Res.* **2009**, *31*, 157–170. [[CrossRef](#)]